Journal of Constructional Steel Research 197 (2022) 107459

Contents lists available at ScienceDirect

Journal of Constructional Steel Research

journal homepage: www.elsevier.com/locate/jcsr

Building retrofit with reduced web (RWS) and beam (RBS) section limited-ductility connections

Afshin Moslehi Tabar [a], Andres Alonso-Rodriguez [b,d], Konstantinos Daniel Tsavdaridis [c,*]

[a] Department of Civil Engineering, Tafresh University, 3951879611 Tafresh, Iran
[b] Institute for Risk and Uncertainty, University of Liverpool, Peach Street, Chadwick Building, L69 72F Liverpool, UK
[c] Department of Engineering, School of Science and Engineering, City, University of London, Northampton Square, EC1V 0HB London, UK
[d] Departamento de Ingeniería Civil, Universidad Católica del Norte, Av. Angamos 0620, Antofagasta, Chile

ARTICLE INFO

Keywords:
RWS connections
RBS connections
IDA
Ductility
Retrofit
Steel frames

ABSTRACT

Softening of beams near the moment connection can be regarded as one of the most convenient methods for retrofitting non-seismically designed buildings. This can be done by drilling the beam web near the connection (aka RWS–Reduced Web Section) or cutting the beam flanges (aka RBS–Reduced Beam Section). Thus, becoming a cost-effective option for retrofitting and erection of new buildings, while optimising use of steel; making the most of this high environmental impactful material. This study presents a comprehensive investigation of the effects of using extended end-plate bolted RWS and RBS connections in building behaviour when subjected to strong ground motion. For that purpose, incremental dynamic analyses (IDA) were performed in a low height building fitted with RWS and RBS connections capable of limited ductility. This was done with the aim of characterising the seismic behaviour of buildings with deficient earthquake design after being subjected to seismic upgrade. It is observed that empirical fragility curves show that probabilities of exceeding 1%, 2% and 4% inter-story drifts are significantly lower (more than 25%) for the building that is designed with RWS connections instead of RBS connections; while the probability of collapse is reduced by at least one third. This indicates that deployment or RWS connections can reduce the risk of both; severe structural damage and, large economical loss due to damage of non-structural elements when seismic demands are moderate.

1. Introduction

Many of legacy buildings may not comply with modern seismic design requirements. Considering the vast distribution of such buildings, the employment of quick and affordable ways for seismic retrofit is of key importance [1,2]. For instance, the use of non-symmetric extended end plates has been predominant in the UK. However, this structural solution is known to display extensive damage and fragile failure modes even when subjected to moderate seismic actions [3]. Complimentarily, softening of beams on locations close to the beam-column interface is one of the most convenient methods for retrofitting of non-seismically designed buildings [4], as shear and moment demands on the beam-column connection are capped. This can be achieved by weakening the beam web by making perforations within it, leading to reduced web section (RWS) or by trimming their flanges (RBS).

Use of perforated beams (aka RWS) is becoming widespread in the UK; where seismic hazard is low. This is due to a number of benefits such as their reduced self-weight; their increased sustainability as the use of steel is optimised; and ease of integration of utilities and supplementary equipment; which can be accommodated through the openings, instead of placed underneath the beams. Consequently, there is extensive research on the structural capacity of RWS beams [5–8] eventually leading to robust guidelines for their use for non-seismic structural applications [9,10].

Undesired behaviour of moment-resistant connections was observed in the aftermath of the 1994 Northridge Earthquake. Particularly, there was extensive inelasticity within and around the connection welding [11]. For that reason, the basic principle for the design of moment-resistant connections changed, precluding plastic behaviour in columns and beam-column joints, while aiming for yielding of the full cross-section of beams instead. On the other hand, inelastic behaviour in properly designed RWS beams is caused firstly by the occurrence of a Vierendeel mechanism where local yielding occurs on the edges of the perforations [12] This divergence in behaviour, coupled with first

* Corresponding author.
E-mail address: Konstantinos.Tsavdaridis@city.ac.uk (K.D. Tsavdaridis).

https://doi.org/10.1016/j.jcsr.2022.107459
Received 28 February 2022; Received in revised form 29 July 2022; Accepted 1 August 2022
Available online 17 August 2022

impressions about how weakening of the web could lead to concurrent non-ductile behaviour like early web buckling, tearing, and torsional failure; resulted in scepticism about the use of RWS connections for applications where ductile behaviour is a critical factor.

However, recent numerical simulations [13] and experimental tests [4] have shown that it is possible to allow for significant inelastic behaviour in RWS connections when subjected to cyclic actions. The Vierendeel mechanism is a reliable option because it caps the shear that can be transmitted from the beam to the beam-column connection, without extreme distortion of the beam web; whilst panels in between perforations still allow for coherent deformation of flanges and webs, thus limiting torsion and buckling [14].

Consequently, use of RWS connections for seismic applications is a plausible option. This can be done in new buildings, but most promising, for retrofitting of non-seismically compliant buildings. Making perforations on the webs (RWS) and flanges (RBS) of beams within steel-frame buildings to cluster inelastic action in protected zones, away from fragile beam-column connections, can be done in a straightforward manner; while upgrading to other solutions involving connection strengthening would require disassembly, making it more costly and disruptive.

For that purpose, this study explores solutions for quick retrofitting of buildings by making changes solely in the cross-section close to the beam-column end; mimicking a quick approach for seismic upgrading, where existing non-compliant connections are kept. For that case, a non-symmetric beam-column connection widely used in the UK is herein considered.

This way, effects on global building behaviour of two cross-section reduction strategies are compared. For that purpose, a 4-storey prototype building was designed and fitted with both types of connections, leading to two distinct models. Then fragility curves for both models, associated with diverse performance objectives conditioned by inter-story drift (threshold of structural damage, moderate damage, extensive damage, and collapse) were computed. Finally, behaviour at collapse was evaluated, focusing on the inelastic displacement amplification at the top along with computation of strength reduction factors.

2. Study framework

This study extends a research initiative that assessed experimentally the performance of beams with reduced web (RWS) and reduced flanges (RBS) of beam-column connections [4]. For that purpose, a prototype four-storey steel building is formulated. Non-symmetric end-plate connections within it are retrofitted by reducing beam web or beam flanges, thus migrating inelastic demands from the beam-column interface. Then seismic response of the prototype to far-field ground motions is investigated by performing analysis in commercial structural engineering software.

Suitably of the analytical framework is verified by replicating the results of the experimental testing campaign [4]. This led to the development of a simplified lumped plasticity model to represent the behaviour of RBS and RWS connections with non-seismically compliant end plates. Then properties of the beam and columns of the 4-storey steel prototype building are defined in accord to AISC specifications (2016). Consequently, the obtained structural elements are connected using both RWS and RBS connections assessed in [4], leading to two distinct prototypes. Afterwards, a representative middle-bay moment frame was selected to be subjected to Incremental Dynamic Analyses (IDAs) for each prototype. Finally, the results of the IDA analyses become the input for computation of fragility curves that allow for comparison of performance of both types of connections.

2.1. Veriffcation study and development of the beam-column analytical model

This study compares two strategies for improving the seismic performance of non-symmetric top-side extended end-plate beam-column connections using RBSs and RWSs. The former approach involves making cuts on the beam flanges to create a protected zone where extensive yielding can take place, thus ensuring that inelastic action occurs away from the beam-column connection [15–19]. As an alternative, the RWS approach involves cutting or allocating perforations on the beam web to induce the formation of a Vierendeel Mechanism [20,21] that leads to stable shear yielding when subjected to cyclic actions, precluding inelastic behaviour on the beam-column edge. As shown in Fig. 1, only one hole is provided near the column face for the RWS. Previous research has benchmarked both solutions via laboratory testing [4].

Firstly, an analytical representation of the connection is proposed. For that objective, a lumped plasticity approach is considered [22]. Thus, all inelastic action is expected to occur on the beam's protected zone (around and over the perforation). Specifically, three rotational springs are arranged in series as shown in Fig. 2. The first one models the flexibility of the shear panel in the column, which is assumed to remain elastic. The second one represents the interaction at the beam-column interface. The third one is a symmetric plastic hinge that simulates the protected zones in both the RWS and RBS connections.

According to Fig. 3, the rotational stiffness of the first hinge can be derived as follows:

$$V_{PZ} = \frac{GA}{d_b}\delta_{PZ} = GA\,\theta_{PZ} \tag{1}$$

After multiplying both sides of Eq. (1) by d_b, it becomes:

$$K_{PZ} = GAd_b \tag{2}$$

Where, K_{PZ} is the rotational stiffness of the column panel zone, G is the shear modulus of steel (80GPa), A is the column web cross-sectional area and d_b is the beam depth. Eq. (1) provides a simplified way to account for the elastic shear distortion of the panel zone.

The second spring models slippage and deformation on the beam-column interface. Although the end-plates used as the beam-column interface are the same in the RWS and RBS models, two distinct approaches were used for representing their behaviour (Fig. 4). For the RWS a friction link with a positive post-yield slope is considered, as shown in the figure. This allows for partial decoupling of the beam-column interface. On other hand, the RBS is modelled using a friction link with a flat post-yield slope, thus enhancing supplemental beam-column interface deformation induced by buckling and torsion of the RBS beam; which is a consequence of its reduced torsional stiffness due to flange trimming [4]. The difference between the performance of the end-plates used in the RBS and RWS models can readily be observed from Fig. 5.

Although both RBS and RWS exhibited comparable pre-yield stiffnesses, their behaviour after yielding diverges. The RBS specimen displayed slippage, which became the dominant trend as it becomes sensitive to out-of-plane stability; whilst the RWS showcased in-plane flexure-related plate deformation.

The second spring follows the trilinear stiffness degrading Takeda model [23]. Albeit this model is widely used for representing the behaviour of concrete elements, its ability to model pinching and stiffness variation with deformation made it a suitable choice to represent traits observed during testing of RBS and RWS connections with non-symmetric beam-column connections. The Takeda model is similar to the kinematic model except that in the reloading stage, the curve follows a secant line to the backbone curve for loading in the opposite direction. The target point for this secant is at the maximum deformation that occurred in that direction under previous load cycles.

Finally, moment-rotation relationships in the protected zones (RBS or RWS) are idealised using yielding hinges in accord with what is prescribed in FEMA 356 [24]. Their backbone curves are shown in Fig. 6. The only difference amongst RWS and RBS representations is the rotation thresholds. For both cases, the yielding moment is calculated

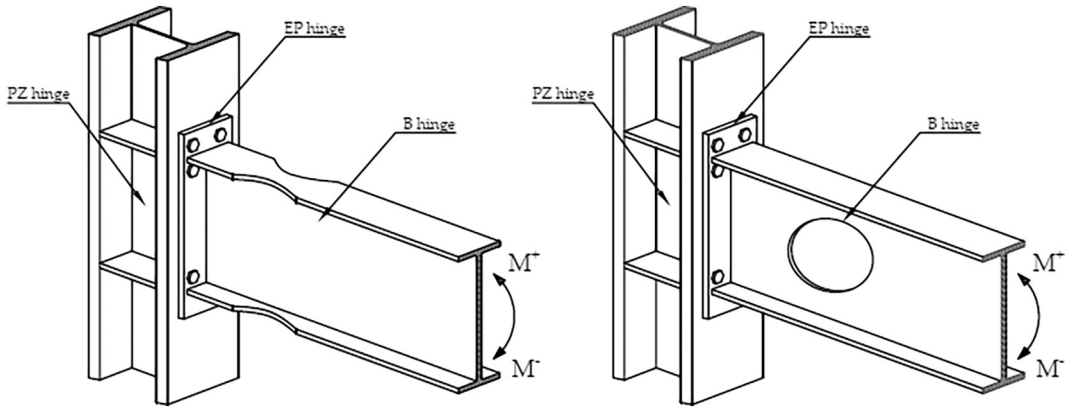

Fig. 1. Steel moment connections considered in this study: RBS connection (left), RWS connection (right).

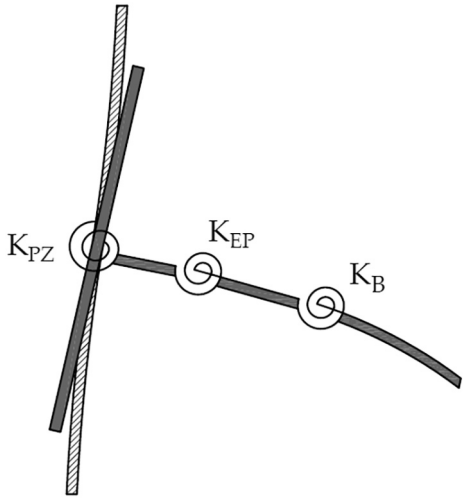

Fig. 2. Schematic arrangement of the rotational springs.

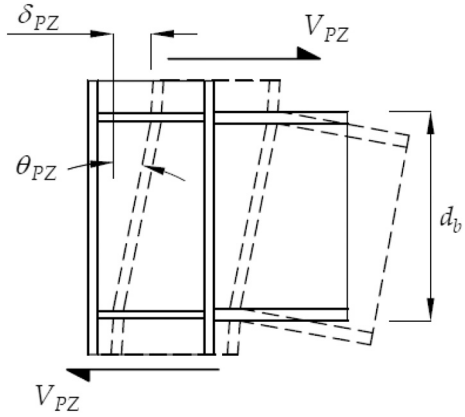

Fig. 3. Deformation of the column panel zone.

considering the reduced cross-section and the capacity of the Vierendeel mechanism [4].

Experimental benchmarking data for this study is based on tests done by Tsavdaridis et al. [4]. They subjected RWS and RBS beam-column connections typical in the United Kingdom to displacement-controlled cyclic actions. As the UK is a low earthquake hazard region, the connections lacked capacity design detailing, showcasing features like non-symmetrical beam-to-column connections. However, similar detailing can be observed in regions where building code compliance is sparse, as expected in the Global South.

Results from the tests indicate that RWS connections were less sensitive to lack of proper seismic detailing than their RBS counterparts, even reaching 4% interstorey drifts without showcasing fragile failure modes like connection-tearing, web-buckling, and large deformation within the end-plate, whilst being capable of describing stable hysteresis loops. Contrarily, RBS specimens displayed extensive end-plate deformations due to the loss of restrain provided by flange trimming. Further details about the experiments can be found in [4].

Tests were simulated in ETABS [25], and it was found that the numerical scheme replicates major observed phenomena: stiffness degradation, pinching and non-symmetrical features of backbone curves, particularly for the RBS connection.

Results in [4] show that both beams have similar positive (sagging) yielding moment capacities, close to 130kN, which were recorded at similar chord rotations. The numerical results follow to the tests in this regard, as shown in Fig. 7. In this figure, the rotation is the whole chord rotation of beam.

In order to better justify how different hinges, contribute to the total response, the moment-rotation diagrams related to the rotation of the beam hinge (rotation in RWS or RBS connections) and the end-plate connection (rotation due to the end-plate deformation) are shown in Figs. 8 and 9 for RWS and RBS connections, respectively.

Comparing Figs. 8 and 9 with Fig. 7, it is inferred that the general behaviour of each specimen is mostly dominated by the beam plastic hinges.

Once the models have been verified, it is useful to characterise the hysteretic behaviour prior the allocation of either RWS or RBS connections. For this purpose, a new model of a connection without beam weakening was generated, but the non-symmetric extended end-plate connection was kept. Hysteretic behaviour of this model is depicted in Fig. 10.

Comparing Figs. 10 and 7, it is clearly observed that the specimen without beam weakening leads to non-symmetrical hysteresis loops with low energy dissipation, along with limited plastic rotation when positive (sagging) moments are applied. Contrarily, the retrofitted specimens (especially the one fitted with RWS connections) display a more desirable behaviour, leading to stable, symmetrical hysteresis loops without pinching or origin wandering (deformation reversed almost completely with the load) but allowing for large energy dissipation, as reflected on the larger enclosed area within each cycle.

For better justification, the energy dissipated during a complete excursion of 0.03-rad total rotation in the models, and their corresponding plastic rotations are evaluated as given in Table 1. As observed, the RWS model showcases superior performance and obviously overperforms when compared to the original model. The RBS connection increased the plastic rotation although it has the least energy

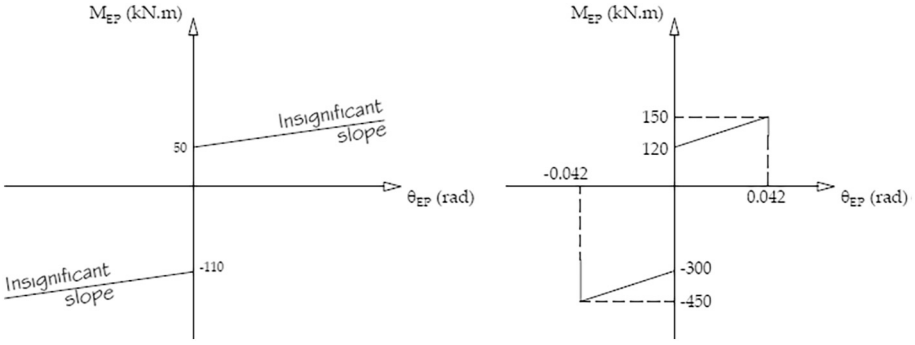

Fig. 4. Modelling of the beam-column interface: RBS connections (left), RWS connection (right).

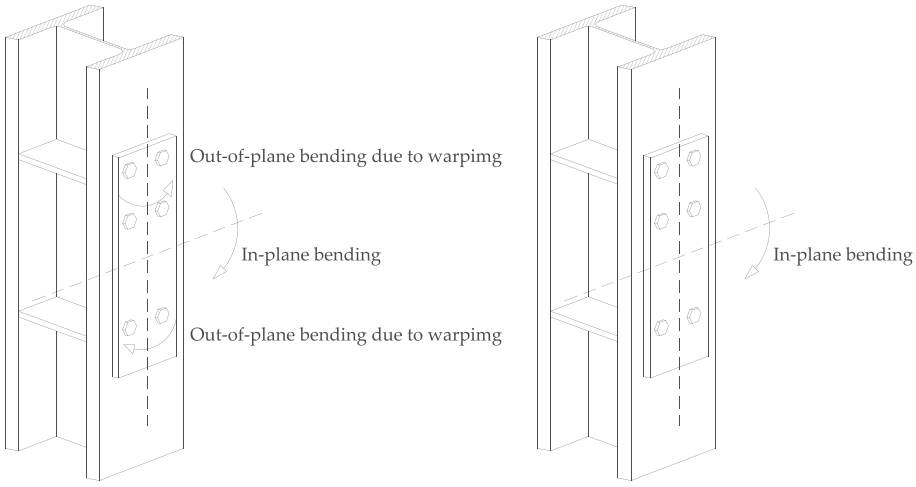

Fig. 5. Performance of the end-plate in: RBS connections (left), RWS connection (right).

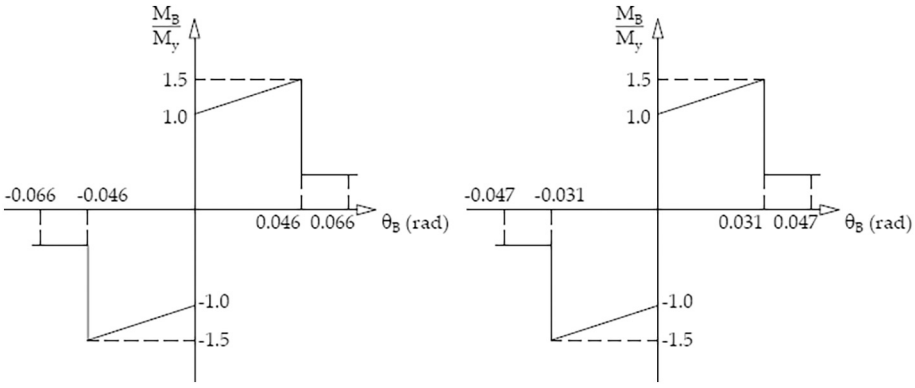

Fig. 6. Modelling of the beam plastic hinge: RBS connection (left), RWS connection (right).

dissipating capability. The RWS and RBS models satisfied the minimum plastic rotations, required for Special and Intermediate Moment Frames according to AISC [3].

3. Analysis methodology

The methodology employed in this study is incremental dynamic analysis (IDA). It was firstly, formulated by Vamvatsikos and Cornell [26], and it involves effectuating linear and non-linear numerical analyses on a structural model, considering a collection of strong motion records that are successive scaled until collapse, which is defined as lack of convergence of the numerical model as a failure mode develops and the vertical load-carrying capacity is compromised. These ground motion records should reflect features expected on the frequency content of the site shaking. Then, it is possible to study the response of the ensemble of results to judge if the structure complies with desired performance objectives following the performance-based design philosophy (PBD). PBD aims to limit non-structural damage and allow for quick repair and operation when ground strong motion intensity is low whilst minimising the extent of structural damage and the possibility of collapse when seismic demand is high. For further details on PBD the reader is referred to FEMA 445 [27]. All analyses were done in ETABS.

The most typical way to assess structural performance within the PBD framework is through fragility functions. They specify the

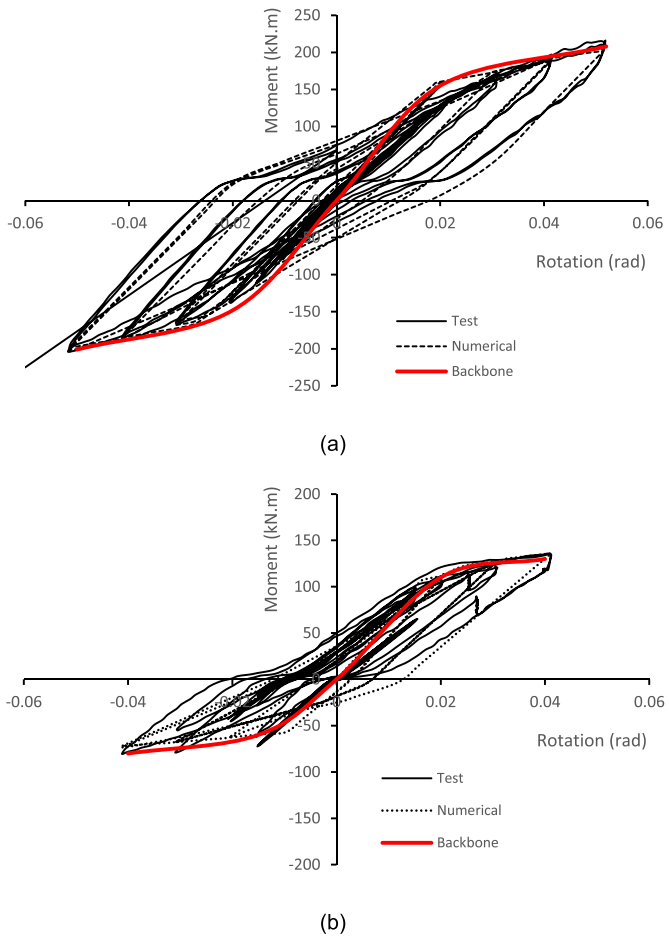

Fig. 7. Replication of experimental benchmark test for studied: (a) RWS; and (b) RBS.

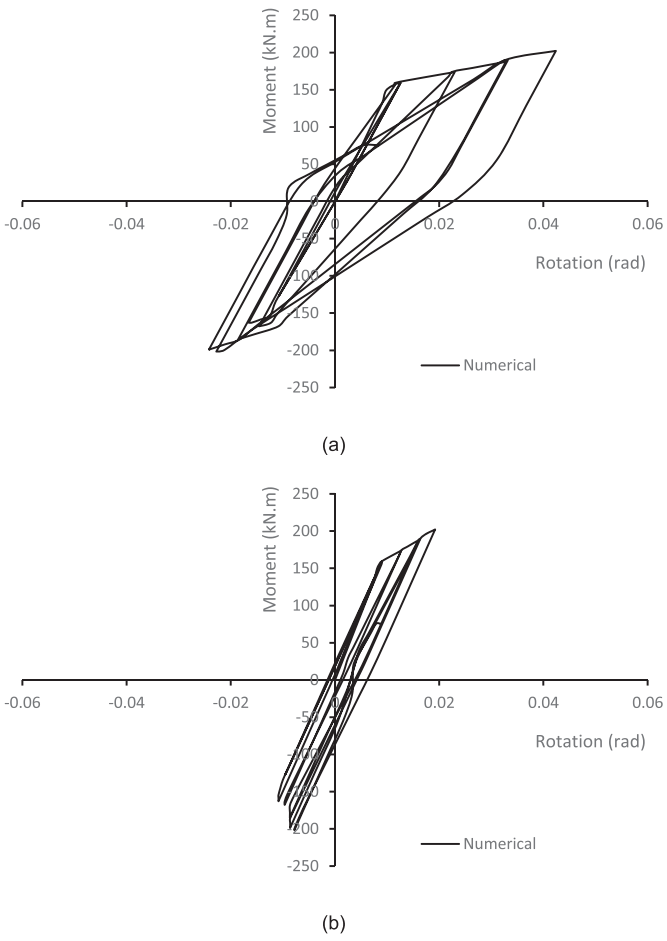

Fig. 8. Moment-rotation diagrams of: (a) Beam hinge and (b) end-plate connection for RWS specimen.

probability of observing a damage state (normally structural damage) conditioned on achieving a particular engineering ground motion intensity. It is a common practice to relate these damage states to structural engineering demand parameters; being peak floor acceleration [28] and inter-story drift [29] the prime options. The most widely used ground motion intensity employed is PGA. However, PGA does not convey information about the building characteristics. The spectral acceleration response at the fundamental period is the benchmarking ground motion parameter in this study. This is a sensible selection as the response of low and moderately tall buildings is dominated by the fundamental period.

3.1. Ground motion ensemble considered

This study employed the far-field set compiled in FEMA P695 [30] for defining the ground motions employed to characterise seismic demands associated with far-field ground motion. As it can be seen in Table 2, Richter magnitudes range between 6.0 and 7.5; and records arise from inter-plate events on land. Large subduction earthquakes were excluded, due to their long frequency content. Likewise, events observed at epicentral distances larger than 100 km were also neglected, as the focus is made on strong motion that can potentially generate extensive structural damage. This leads to a wide range of PGAs, as shown in Table 2.

It must be stressed that ground motion variability caused by earthquake events is large for both inter (amongst diverse events) and intra (within the same event) records, as surface response is affected by diverse phenomena, amongst them; site conditions, directionality, boundary conditions on the surface, etc. Consequently, it is possible that acceleration records that were generated by a single fault rupture may denote distinct features that can affect diverse structures differently. Thus, it is reasonable to include records associated with the same earthquake event, as long as their frequency content, duration and single-parametered instrumental intensity (usually measured in term of PGA and PGV) are varied.

The collection of response spectra associated with the grouped strong motion records is shown in Fig. 11. Most relevant acceleration response is observed for periods less than 1 s which is more than what is expected for the fundamental period of the building prototype being assessed. Yet, the ensemble showcases a varied response, enough to assess the behaviour of the model to diverse conditions.

3.2. Prototype building

The prototype building is a four-story structure for residential use with bay width spanning 6 m in both directions, while the typical floor height is 3 m and the first level is just 2.4 m as it is used as a garage. Allocation of structural elements follows what is stated in the AISC 360 [31] guidelines. As previously mentioned, the connections are comprised by non-symmetric extended end-plates. They are commonly observed in ageing buildings in the UK, and it is common practice to consider them rigid whilst enduring gravitational loads. This feature is also likely to be found in buildings with poor seismic detailing, where capacity design principles are not tightly enforced. The baseline seismic demand level for design corresponds to a PGA with a return period of 475 years, associated with a 10% probability of exceedance in the

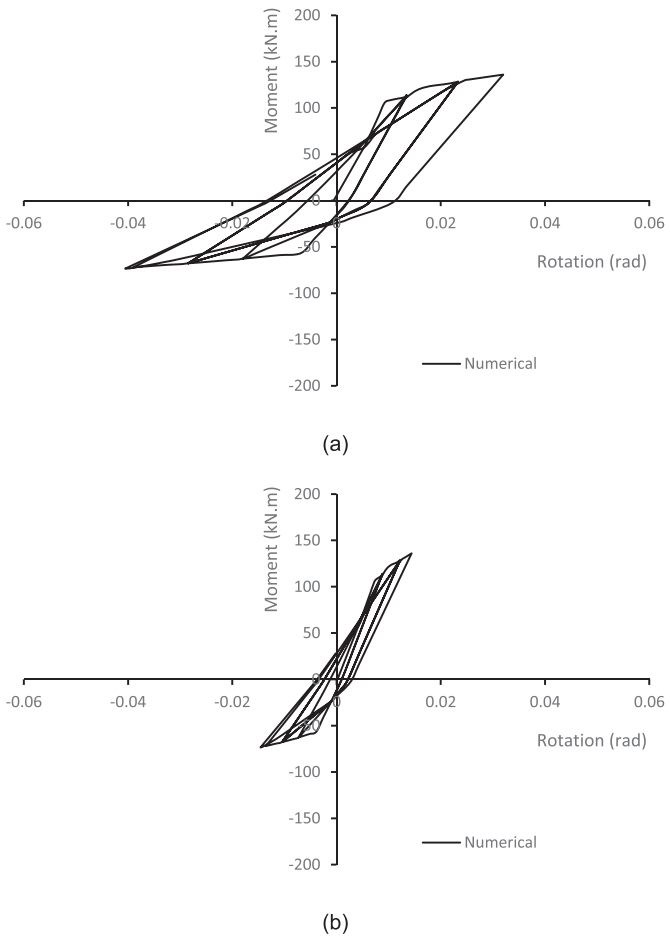

Fig. 9. Moment-rotation diagrams of: (a) Beam hinge and (b) end-plate connection for RBS specimen.

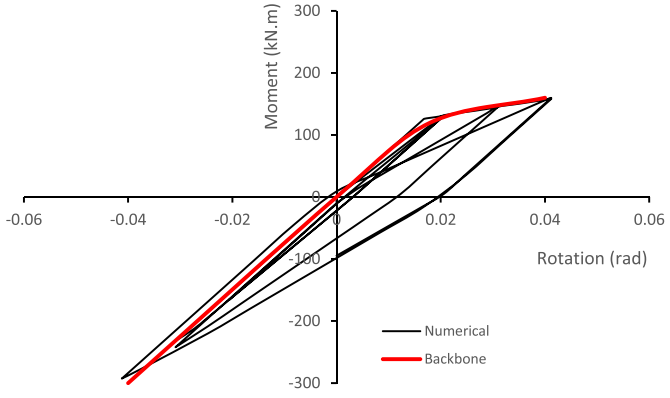

Fig. 10. Predicted behaviour of the original specimen before retrofit.

Table 1
Evaluation of structural properties of the models.

Model	Energy dissipated (kN.m)	Plastic rotation (+) (rad)	Plastic rotation (−) (rad)
Original	2.3	0.022	0
RWS	3.0	0.033	0.033
RBS	2.1	0.025	0.028

Table 2
Strong motion records employed in this study.

Year	Name	Station	Magnitude [Richter]	Epicentral distance [km]	PGA [g]
1994	Northridge	Beverly Hills – Mulhol	6.7	13.3	0.52
1994	Northridge	Canyon Country-WLC	6.7	26.5	0.48
1999	Duzce, Turkey	Bolu	7.1	41.3	0.82
1999	Hector Mine	Hector	7.1	26.5	0.34
1979	Imperial Valley	Delta	6.5	33.7	0.35
1979	Imperial Valley	El Centro Array #11	6.5	29.4	0.35
1995	Kobe, Japan	Nishi-Akashi	6.9	8.7	0.51
1995	Kobe, Japan	Shin-Osaka	6.9	46.0	0.24
1999	Kocaeli, Turkey	Duzce	7.5	98.2	0.36
1999	Kocaeli, Turkey	Arcelik	7.5	53.7	0.22
1992	Landers	Yermo Fire Station	7.3	86.0	0.24
1992	Landers	Coolwater	7.3	82.1	0.42
1989	Loma Prieta	Capitola	6.9	9.8	0.53
1989	Loma Prieta	Gilroy Array #3	6.9	31.4	0.56
1990	Manjil, Iran	Abbar	7.4	40.4	0.51
1987	Superstition Hills	El Centro Imp. Co.	6.5	35.8	0.36
1987	Superstition Hills	Poe Road (temp)	6.5	11.2	0.45
1992	Cape Mendocino	Rio Dell Overpass	7.0	22.7	0.55
1999	Chi-Chi, Taiwan	CHY101	7.6	32.0	0.44
1999	Chi-Chi, Taiwan	TCU045	7.6	77.5	0.51
1971	San Fernando	LA – Hollywood Stor	6.6	39.5	0.21
1976	Friuli, Italy	Tolmezzo	6.5	20.2	0.35

following 50 years. It has been hypothetically placed in an area underlain by a site C according to ASCE-7 [32], and consequently the design PGA is 0.30 g. Designed RBS and RWS connections have the same flexural stiffness before yielding.

The earthquake resistance structural system is comprised by perimeter single-bay braces and moment-resisting frames acting on orthogonal directions across all spans. Gravity elements lean on the braces while the moment-resisting frames also support vertical loads, as shown in Fig. 12.

As the purpose of this study is to understand the difference in behaviour when providing RWS or RBS connections, 3D effects are secondary and could introduce noise in the assessments, whilst significantly increasing complexity. Therefore, the frame on the B axis was selected for benchmarking, focusing on in-plane analyses (Fig. 13). This choice was made because all frames in the longitudinal axis are part of the lateral load resistance system. Thus, inner frames are the most common in the building whilst carrying the largest share of both vertical loads and floor shear.

Besides the plastic hinges representing the RBS and RWS connections at the end of each beam, supplemental force-controlled hinges were allocated at the end of each column to allow for degradation of the column load-carrying capacity. Moreover, it should be highlighted that effects on slabs were not addressed in this study as experimental data in this regard is limited.

It should be noted that for the beams used in the prototype building (CPE360 and CPE400) the flanges cut in RBS and the hole diameter in RWS have, approximately, the same ratio as those used in Ref. [4], i.e., 50% cut of flanges for RBS and provision of hole with a diameter of 75% the section depth for RWS.

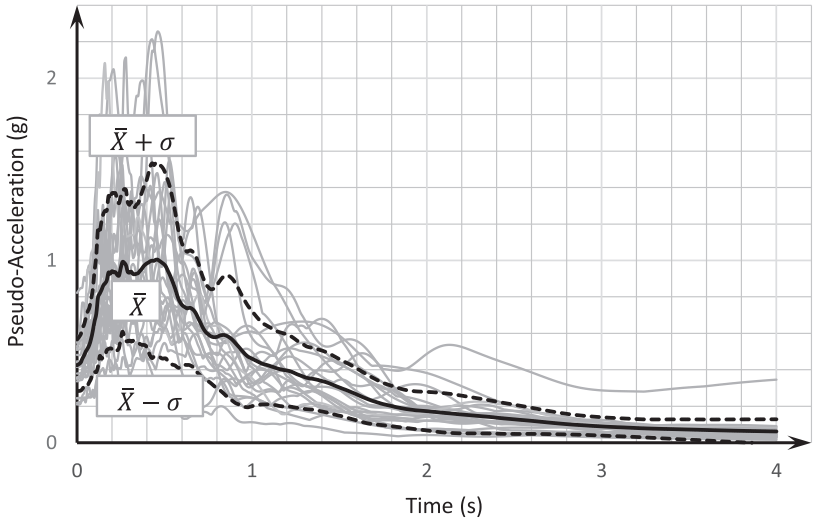

Fig. 11. Response spectrum of the unscaled records, indicating mean values, plus and minus 1σ (standard deviation) limits.

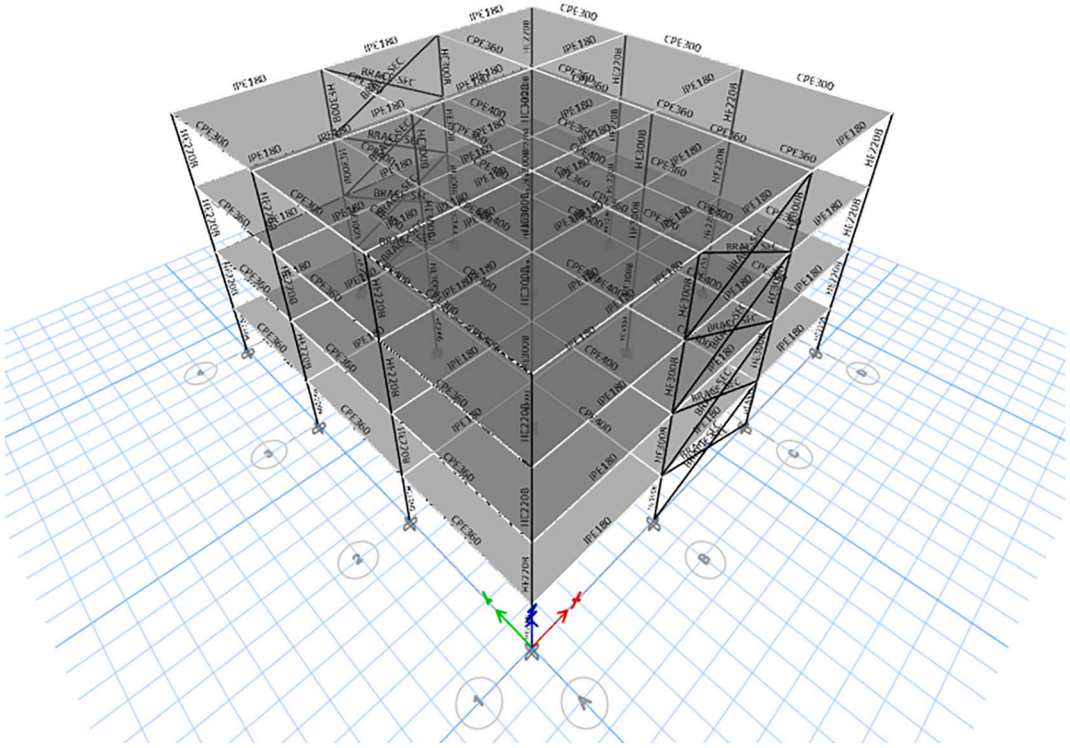

Fig. 12. 3D view of the 4-story frame associated with the designed element sections.

3.3. Modal properties of prototype building

The fundamental period of the prototype building is 0.66 s, which is 4% larger than the mean value suggested by empirical height, fundamental-period relationships [33] used for structural design [32]. Consequently, the approach presented in this study leads to structures that are representative of what is observed in practice.

$$T_1 = 0.091H^{0.8} \tag{3}$$

Where, T_1 is the fundamental (first) mode period in seconds, and H is the building height in metres. Higher-mode periods are presented in Table 3, where they are compared to what is observed for a fixed-base cantilevered shear beam with the same fundamental period. The agreement is close on the second mode, where the value for the building is 4% for the first and second modes, while they are slightly less than 20% for the third and fourth modes. It should be noted that as the focus of this paper is on assessing the behaviour of both connection types (RBS and RWS) when allocated in the lateral load resistance system; both cases were designed to have the same nominal moment capacities and showcase the same pre-yield hogging stiffnesses. Consequently, both building models have the same elastic modal periods and modal shapes.

Modal periods and shapes are benchmarked against a continuous surrogate shear beam model (Fig. 14), which represents reasonably well the seismic behaviour of high-rise buildings with moment-resistant frames [34]. Continuous beam representations as surrogate models are useful because they provide a universal model that allows for assessment of large building portfolios, as their response can be described by few parameters, whilst providing general scaling laws. This is particularly

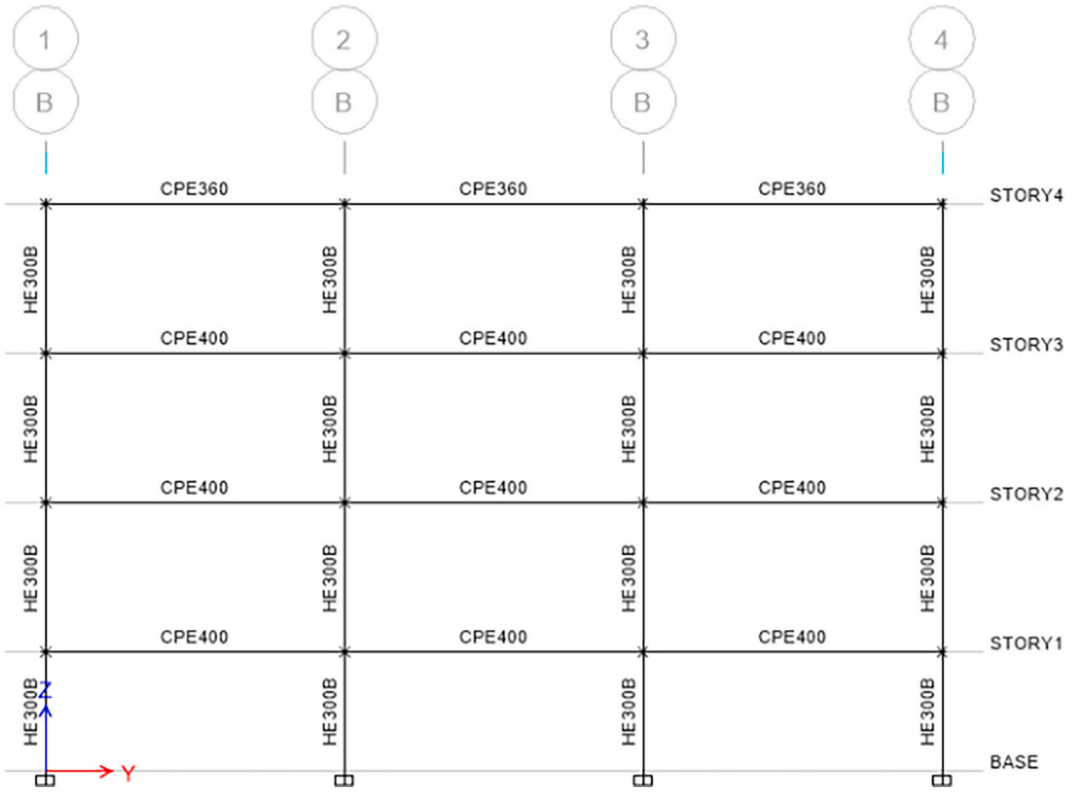

Fig. 13. Typical interior moment frames of the 4-story frame associated with the designed element sections.

Table 3
Modal Periods of the prototype building [s].

Mode	Building	Shear Beam
1st	0.66	0.66
2nd	0.21	0.22
3rd	0.11	0.13
4th	0.08	0.09

useful for earthquake risk assessment of large urban areas.

Modal shapes closely agree on the ordinate at the top of the building. The first mode ordinate is 5% larger than what is observed for the shear beam, while for the second mode, values for the building are 5% lower. Nevertheless, mode shapes diverge significantly for other locations. Clearly, the number of levels is too low to make the analogous shear beam model reliable at locations different than the last level.

4. Results

4.1. Fragility curves

Empirical fragility curves display the conditional probability of exceeding a particular structural demand given that a strong motion parameter has not exceeded a threshold. Therefore, they provide a direct assessment of the reliability of a structural system. In this study, the selected structural demand parameters are: inter-story drift and occurrence of collapse. The strong motion parameter that characterises the seismic demand is the spectral acceleration at the fundamental period of the structure.

$$F(Sa(T_1)) = P\left(\frac{d > Di}{Sa(T1)\langle Sa(T_1)_i}\right) \tag{4}$$

Where, F is the fragility distribution function, $Sa(T_1)$ is the spectral acceleration at the fundamental period, d is the inter-story drift, D_i is the

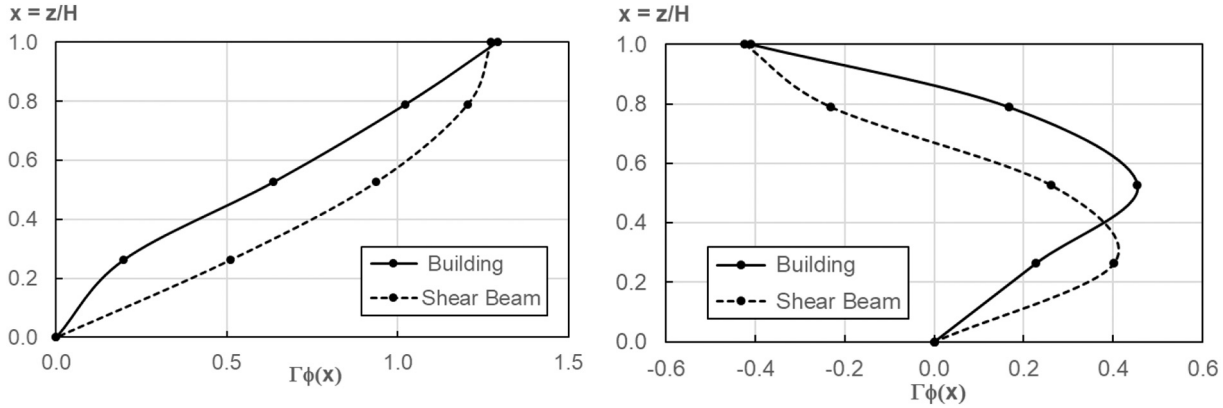

Fig. 14. First and Second mode shapes of the prototype building, benchmarked against a continuous shear beam.

drift threshold being considered in the analysis, and $Sa(T_1)_I$ is the spectral acceleration limit. Bayes theorem allows for Eq. (4) to be rewritten as:

$$F(Sa(T_1)) = \frac{P\left(\frac{Sa(T1)\langle Sa(T_1)_i}{d>Di}\right)P(d > Di)}{P\left(a(T1)\langle Sa(T_1)_i\right)} \quad (5)$$

The first term in Eq. (5) is the fraction where the $Sa(T_1)$ is lower than the specified limit $Sa(T_1)_i$, amongst those analyses where drift demand is large than the given D_i. The second factor is the ratio of records where drift exceeds D_i to the total number of analysis in the IDA procedure; and the denominator is the fraction the number of records where the spectral accelerations is less than $Sa(T_1)_i$ and the total number of analyses performed. Consequently, Eq. (5) can be computed directly from results.

It must be stressed that conditional probability distributions are being calculated instead of probability density functions; being the latter the most commonly used in risk analyses. However, it is trivial to obtain the latter from the former by taking the partial derivative of the conditional distribution (Eq. (5)) in terms of $Sa(T_1)$.

4.1.1. Drift fragility curves

The fragility curves for drift exceeding 1%, 2%, 4% and collapse are shown in Fig. 15.

For all drift limits considered in this study, RWS connections perform better than RBS connections. This indicates that buildings with the RWS connections are expected to be safer, as they are likely to experience lower drifts than their RBS counterparts, regardless of the seismic demand.

In particular, the probability of initiating structural damage, as indicated by exceeding a 1% inter-story drift is between 2, for $Sa(T_1)$ values less than 0.7 g; to 1.3 times larger for $Sa(T_1)$ values larger than 3; when the RBS connections are considered instead of the RWS ones. For this level of drift non-structural damage is expected to be extensive [35], and consequently, economical losses are going to be significantly larger for the former.

For 2% and 4% inter-story drifts, which loosely correspond to the performance threshold for moderate ductility connections, the ratio amongst probabilities of exceeding the threshold ranges between 2 and 1.2. Being the limits observed for $Sa(T_1)$s of 1 g and 3 g, respectively. Although these values of $Sa(T_1)$ seem high at first sight, it is common to observe strong-motion amplification factors larger than 2.5 in buildings, as usually prescribed by earthquake design codes (ASCE/SEI, 2022 [31]), indicating that even if $Sa(T_1)$ takes values as low as 1 g (which is a moderate shaking), differences on structural damage experienced by buildings fitted with RBS and RWS could be significant.

Finally, RWS connections lead to significantly lower probabilities of collapse. For all $Sa(T_1)$ values assessed, they showcase a conditional probability less than 6%, while their RBS counterparts reach a 15% probability for a $Sa(T_1)$ of one 1 g, and eventually reach a probability of collapse of 20% when it becomes 3 g. This is a significant performance improvement as it is roughly 3 to 5 times less likely to observe collapse for moderate ground motion when RWS connections are employed instead of RBS connections.

4.1.2. Floor acceleration fragility curves

Floor Accelerations (FA) are another critical performance factor to be considered in design. Accelerations in excess of 1 g can lead to significant non-structural damage, particularly in critical support systems like HVAC, utilities like electricity, water provision and disposal, communication infrastructure and suspended ceilings. Thus, even if the structural damage is limited, acceleration-induced damage can be significant enough to compromise function and even lead to loss of life [36].

Results, displayed in Fig. 16 indicate that floor accelerations will significantly exceed the spectral response values at the fundamental period. For example, median values for floor accelerations of 0.7 g and 1 g, are observed for Sa(t1) ordinates of 0.85 and 1.5 g, respectively. The uneven ratio amongst these quantities (0.85/0.75 and 1.5/1.0) indicates that single-mode analyses are not well suited to capture floor

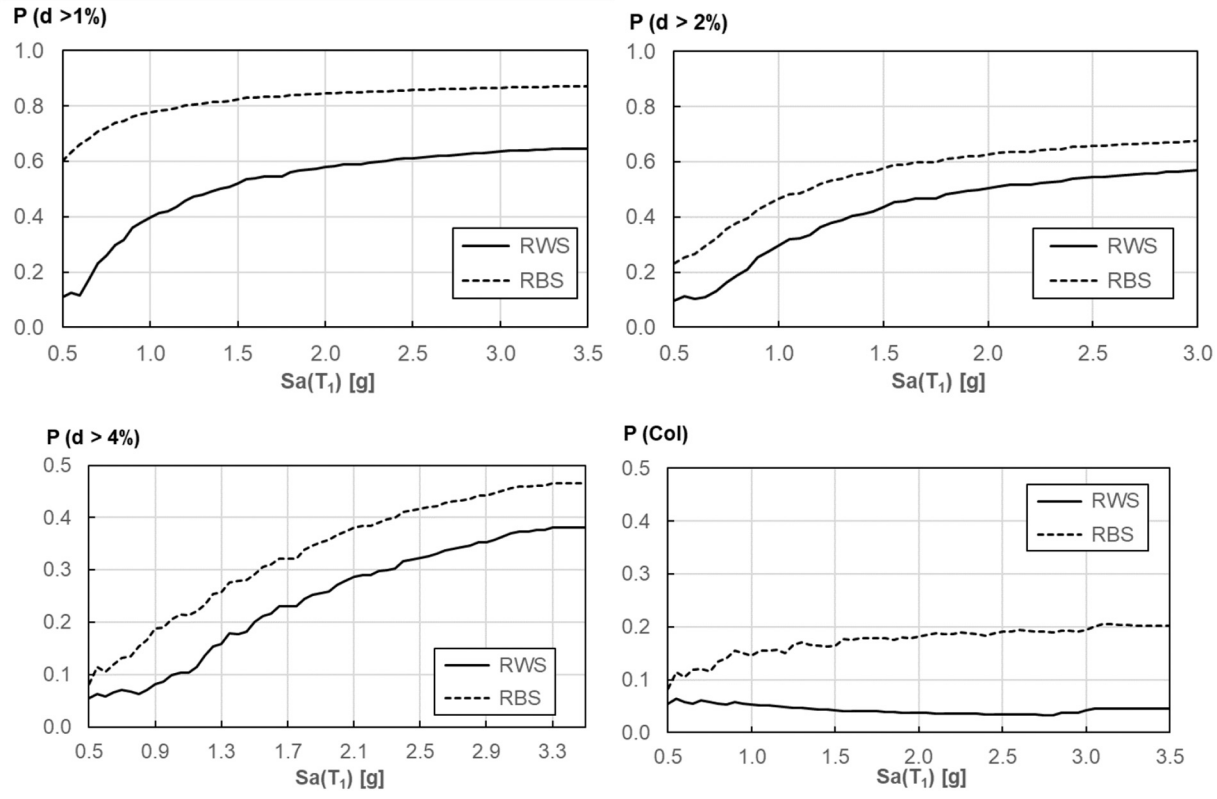

Fig. 15. Empirical fragility curves for drifts exceeding 1, 2, and 4%; and collapse.

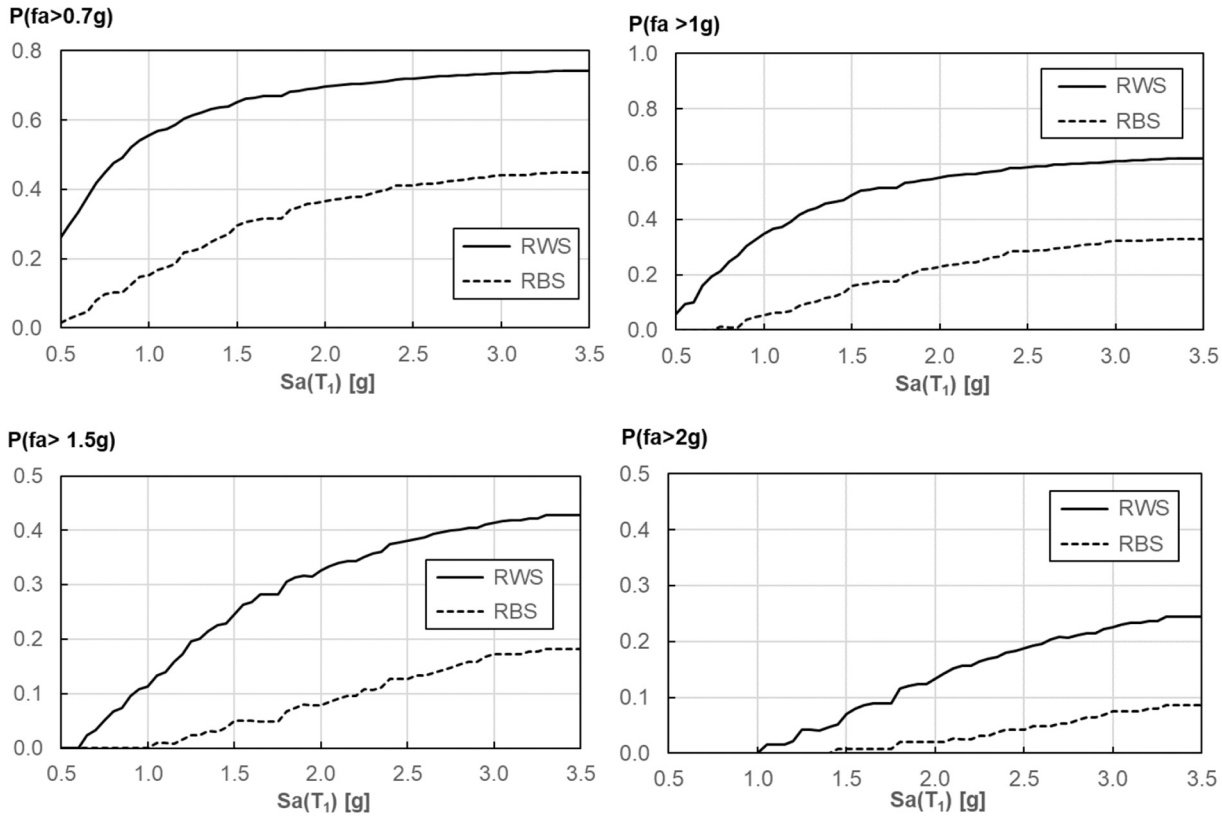

Fig. 16. Empirical fragility curves for floor accelerations exceeding 0.7, 1, 1.5 and 2 g.

acceleration response factor, issue that has been highlighted before [37].

For all assessed FAs the model with RWS connections showcases larger probabilities of exceeding them for most Sa(T1) ordinates, when compared to what is observed with the model with RBS connections. Clearly, the RBS model displays extensive non-linear demands and early collapse as presented in the previous section. This factor limits the extent of the accelerations that can be reached inside the building. Contrarily, better performance exhibited by the RWS connections leads to larger accelerations within the building. This indicates that effective structural seismic retrofitting should include reliability assessments of acceleration-sensitive components

4.2. Inelastic displacement ampliffcation

Inelastic displacement amplification was assessed in the IDA step immediately before collapse, leading to lower bound estimates of inelastic displacement amplification and strength reduction. Histograms for the former are shown in Fig. 17.

Particularly, the displacement at the top of the building was compared to the displacement observed in a model where non-linear behaviour was precluded by considering linear moment-rotation relationship in the model hinges as described by Eq. (6).

$$c_{di} = \frac{dtop_e}{dtop_i} \tag{6}$$

Where, C_{di} is the inelastic displacement amplification factor at the top, $dtop_e$ is the maximum displacement of the elastic model at the roof, and $dtop_i$ is the displacement of the model, in the step before collapse. Amongst all the assessed time histories, collapse of the RWS model was observed in 11 of the 22 ground acceleration time histories considered. While for the model with RBS connections it occurred amongst 17 cases of 22, a ratio of 77%.

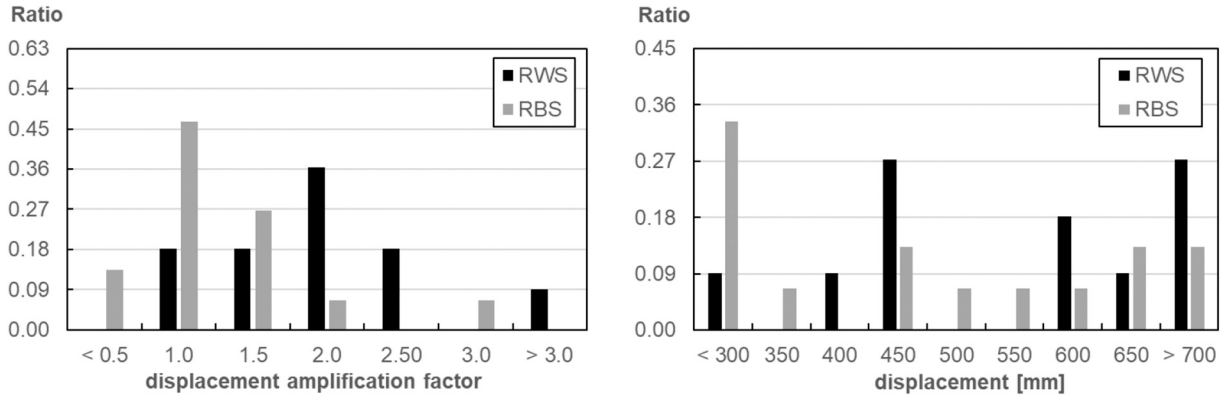

Fig. 17. Histograms of the inelastic amplification factors and inelastic displacement at top.

Summary statistics of C_{di} for both models, with RWS and RBS connections are shown in Table 4. The Student's *t*-test [38] on the means of both populations leads to a *p*-value of 0.056, which is larger than the convention threshold of 0.05, leading to the fact that it is not possible to consider both means to be statistically different for such limit. Clearly, the variability of results for both models is too large to make sound assessments about different behaviours.

However, general remarks can be made by aggregating data. The principle of equal displacements holds as the median value for the whole set is close to 1.0, indicating that the median of displacements of both inelastic and elastic models are similar. Nevertheless, there is a large variability in the data, reflected by a coefficient of variation (ratio between standard deviation and mean) of 0.6.

When considering the largest observed inelastic displacements at the building top (as given in Table 5), there is less confidence about statistically significant divergences between models with RWS and RBS beams. Student's *t*-test [34] *p*-value is 0.28, several times larger than the 0.05 custom limit, which indicates that there is no practical difference amongst both populations. It seems that displacement at top is mostly determined by the characteristics of ground motion.

4.3. Strength reduction factor (R)

As done with the roof deformation, base shear in the step before collapse was studied and compared to what is observed in structures remaining elastic by computing the strength reduction factor, as employed in most structural engineering specifications [36], according to Eq. (7).

$$R = \frac{Vb_e}{Vb_i} \tag{7}$$

Where, Vb_e is the elastic base shear, and Vb_i is the base shear observed before collapse. Summary statistics of R for both models, with RWS and RBS beams are shown in Table 6 while their histograms are presented in Fig. 18. The Student's t-test [38] on the means of both populations yields a p-value of 0.0021, which is less than a full order of magnitude than the convention threshold of 0.05, leading to the fact that it is possible to consider the means of each group to be different with confidence, regardless the observed variability of results amongst each model.

Behaviour of the model with RWS beams is significantly better than the one observed for the model with RBS beams. The median of the former is almost twice the larger, while minimum and maximum values range well above the ones observed for the model with RBS beams. Also, when the standard deviation is normalised by the mean, namely the coefficient of variation (COV). The COV of the model with RWS is lower, (0.3) which is significantly smaller than what is observed for the model with RBS (0.37), indicating that solutions considering RWS elements lead to higher and more reliable reductions in base shear demands in buildings by allowing enhanced inelastic response.

This improvement is due to the significantly larger base shear demands that can be endured by the building model fitted with RWS beams, as clearly shown in Table 7.

Notably, the median ultimate base shear supported by the model with RWS connections is 1.5 times larger than the value observed for the model with RBS connections. Moreover, the minimum base shear sustained for the former is larger than the median value for the latter, indicating how divergent are their behaviours. Likewise, it is notable to mention how the variability of response of the model with RWS connections is almost half what is observed for the model with RBS connections, as represented by the differences on their standard deviations.

These divergences amongst the models are further supported by the fact that the Student's *t*-tests [38] on the means of both populations lead to a *p*-value of 0.003, which, as observed for the R factors, is larger than one order or magnitude that the 0.05 threshold.

Table 4
Summary statistics for Cd_i.

Summary Statistic	RWS	RBS	Both
Maximum	4.12	2.84	4.12
Median	1.55	0.88	1.01
Minimum	0.81	0.42	0.42
Mean	1.71	1.10	1.32
Standard deviation	0.88	0.60	0.80

Table 5
Summary statistics for inelastic displacement at top [mm].

Summary Statistic	RWS	RBS	Both
Maximum	1582	1584	1584
Median	580	431	458
Minimum	291	37	37
Mean	627	466	533
Standard deviation	338	367	364

Table 6
Summary statistics for R.

Summary Statistic	RWS	RBS
Maximum	4.52	2.90
Median	2.83	1.43
Minimum	1.39	0.88
Mean	2.80	1.67
Standard deviation	0.85	0.62

5. Discussion

This study shows how to implement RWS connections with non-symmetrical bolted top side extended end-plates in software used commonly in structural engineering practice. For that purpose, a lumped plasticity approach is proposed. Firstly, the shear induced moment-rotation of the panel zone is represented by a rotational spring. Then it is coupled by a second spring that represents the deformation of the end-plate, while allowing for non-symmetrical early yielding by using Takeda's trilinear stiffness degradation model [23], which is a common choice for assessing the response of reinforced concrete. Then the beam response is assessed by a third spring in series with the previous ones.

Although choice of Takeda's model for representing steel connections is at first sight surprising, it can efficiently represent pinching and stiffness degradation. In concrete, they are both observed due to the deterioration of bonding between rebar and concrete, which leads to buckling of the former in compression and fracture in tension. This process is analogous to the buckling and slippage of bolts in the beam-plate interface. Both were observed in the tests done by Tsavdaridis and his team [4] when studying the response of RWS connections using detailing provided in the UK, a non-seismic region.

If properly detailed symmetrical end-plates are provided, it may be possible to prevent these phenomena and lead to area-stable symmetric hysteresis loops without slippage. Furthermore, if the panel zone is strengthened, for example with doubler plates, its shear deformation can be reduced to a level where it can be neglected in practical terms, thus leading to a simpler formulation where only a single spring is required.

It must be stressed that the development of RBS connections is a top driven approach, in the sense that first solutions were structured to improve behaviour of structures in seismic regions, thus requiring enforcement of proper detailing for enhanced ductility. Therefore, conforming to strong beam-column paradigm is a critical requirement. Contrarily, RWS are widely used in regions where seismicity is sparse, and research is done to explore how they can be adapted to provide enhanced ductility. Clearly, solutions assessed in this study involved beam end-plates that are not expected to be found in buildings with

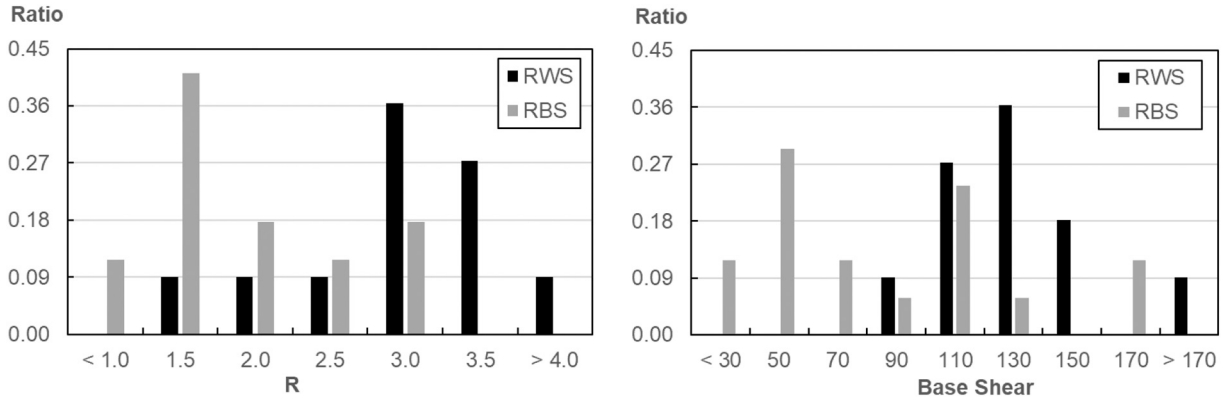

Fig. 18. Strength reduction factor and base shear just before collapse.

Table 7
Summary statistics for Inelastic base shear [kN] before collapse.

Summary Statistic	RWS	RBS
Maximum	174	159
Median	115	76
Minimum	80	66
Mean	118	75
Standard deviation	24	43

proper seismic detailing. Nevertheless, they may be present in structures where enforcement of structural engineering standards is weak, which is usually the case in the global south; or in legacy buildings that haven't been retrofitted.

Results indicate that use of RWS connections with poorly seismically detailed beam end-plates is a better choice than considering their RBS counterparts. Results show an improvement in reducing the probability of occurrence by at least a factor of 2, for a wide range of drifts representing behaviours expected under operational conditions, being the most representative: limited damage, extensive structural damage, and collapse. Thus, this course of action reduces efficiently total expected loss, for both moderate and strong seismic demands, effectively contributing to both life protection and mitigation of total financial loss by reducing drift-related structural and non-structural damage.

Still, improvement in behaviour is limited, as median R factors obtained are slightly larger than 2.75. However, it must be stressed that this result is an outcome for connections with substandard seismic detailing. Results shown by this study are encouraging and make the case of studying the behaviour of RWS connections with more reliable seismic detailing.

Another topic worth of discussion is the collateral effect of increased floor acceleration demands. As RWS connections assessed in this work improve structural behaviour and reduce the probability of collapse, there is a larger chance of enduring larger seismic demands. Thus, floor accelerations that would have not been observed before retrofit, due to early collapse, are now plausible. Structural retrofitting must consider this, as it would be counterproductive to enhance deformation and drift capacity to lead to floor-acceleration driven damage. Results of this study show that improvements on the overall structural behaviour must be coupled with assessments and enhancements of performance of acceleration-sensitive equipment and non-structural elements within the building.

6. Concluding remarks

This study shows how an array of three rotational springs can represent the behaviour of RWS and RBS connections with highly deformable and weak beam end-plates. The approach proposed was implemented efficiently in commercial software used commonly around the globe for structural engineering. Moreover, it uses formulations that are established in guidelines for seismic designs formulated by FEMA. This provides a quick way for use by the overall steel structural engineering community.

The proposed approach was tested by performing IDA analyses in a prototype low-rise building representing structural systems predominant in the Global South, but particularly in the Middle East. Both RBS and RWS connections were assessed finding that provision of the latter reduces the probability of collapse by at least a factor of 4 for spectral accelerations for the first mode larger than 1 and less than 3.5 g. Moreover, reductions larger than 1.5 were obtained for drift demands of 4%, 2% and 1% indicating that use of RWS connections instead of RBS connections also limits interstory-drift driven structural and non-structural damage.

Improved behaviour is further validated by significantly statistical differences on behaviour of both models, with RWS and RBS connections. The first one reached a mean R factor of 2.8, while the latter only achieved a mean value of 1.43. Furthermore, the coefficient of variation of the R factor for the model with RWS connections is 0.3, while for the RBS model is 0.38, indicating that the former provides a more reliable solution, as dispersion of results, normalised by their mean, is relatively lower. Regarding displacements, there is no statistical footing to consider that displacement amplification at the top-level is distinct amongst both groups.

Consequently, providing RWS connections on buildings that do not conform to sound seismic standards, can increase seismic performance as indicated by the obtained R factors, which showcase a median value of 2.8. However, there is scope to improve behaviour by limiting bolt and plate deformation and buckling, curtailing pinching and slippage, eventually leading to an approach with even better performance, capable of achieving enhanced ductility and even larger R factors. On the other hand, the observed poor performance of building seismic response when RBS connections are employed indicates that adaptation of this solution to cases where seismic detailing is not stringent, is unlikely to succeed.

Declaration of Competing Interest

We have no conflicts of interest to disclose.

Data availability

No data was used for the research described in the article.

Acknowledgements

The authors would like to acknowledge funding provided by the

IMAWARE initiative, which supported wages for Dr Alonso-Rodriguez. IM AWARE is funded by the Economic and Social Research Council of the UK (Grant number: ES/T003537/1).

Appendix I. Notations

The following symbols are used in this paper:
A = column web cross-sectional area.
C_{di} = inelastic displacement amplification factor at the top.
d = inter-story drift.
d_b = beam depth (mm).
$dtop_e$ = maximum displacement of the elastic model at the top.
$dtop_i$ = displacement of the model at the step before collapse.
D_i = drift threshold.
G = shear modulus of steel (80GPa).
H = building height.
K_B = rotational stiffness of the beam plastic hinge.
K_{EP} = rotational stiffness of the extended end-plate connection.
K_{PZ} = rotational stiffness of the column panel zone.
M_B = beam moment at plastic zone.
M_Y = plastic moment at plastic zone.
M_{EP} = beam moment at column face.
R = strength reduction factor.
$Sa(T_1)$ = spectral acceleration at the fundamental period.
T_1 = fundamental (first) mode period.
V_{PZ} = shear in column panel zone.
V_{be} = base shear in a model where hinges allow for a linear relationship amongst moment and rotation.
V_{bi} = shear observed for the same ground motion in the models at the step before collapse.
δ_{PZ} = lateral distortion of column panel zone.
θ_B = beam rotation.
θ_Y = beam yield rotation.
θ_{PZ} = rotation of column panel zone.

Appendix II. Sample calculation of the end-plate capacity

According to the geometry details given in Ref. [4] and the guidelines noted in AISC 358 [39] for calculation of the end-plate moment capacity, the negative moment (hogging) capacity of the end-plate is derived as follows (the notations here are the same as those defined in AISC 358 [39]):

(1) For the RWS model:

- *In case of the bolt failure:*

$$M_{bp} = 2P_t(h_0 + h_1) = 2 \times 100000 \times 3.14(29.5 + 20) \times 10^{-3}/9.81 = 320\ kN.m$$

- *In case of the end-plate failure:*

$$s = \frac{1}{2}\sqrt{20 \times 12} = 7.7\ cm$$

$$y_p = \frac{20}{2}\left[24.25\left(\frac{1}{4.25} + \frac{1}{7.7}\right) + 33.75\left(\frac{1}{4.25}\right) - \frac{1}{2}\right] + \frac{2}{12}[24.25(4.25 + 7.7)\,] = 210\ cm$$

$$M_{pl} = 3440 \times 2^2 \times 210 \times 10^{-3}/9.81 = 300\ kN.m$$

- *In case of the column flange failure:*

$$y_c = \frac{20.6}{2}\left[(24.25 + 33.75)\left(\frac{1}{4.25} + \frac{1}{7.7}\right)\right] + \frac{2}{12}[(24.25 + 33.75)(4.25 + 7.7)\,] = 333\ cm$$

$$M_{cf} = 3440 \times 1.73^2 \times 285 \times 10^{-3}/9.81 = 340\ kN.m$$

Thus, the negative plastic moment capacity of the connection is taken as 300 kN.m as shown in Fig. 4. The ultimate moment capacity in this situation is taken as 400 kN.m which considers the effect of a 3% strain hardening factor, in accord with FEMA 356. In contrast, for the positive moment (sagging) capacity the plastic moment capacity is derived as 120 kN.m which is less than half of that in negative moment. This is due to the fact that only a single row of bolts is provided.

Moreover, as the plate yielding dominates the connection performance, the rotation capacity of the end-plate is considered 0.042 rad based on FEMA 356.

(2) For the RBS model:

According to the experimental study in Ref. [4], a major slippage was observed in the RBS model due to the beam lateral-torsional buckling accrued soon after the RBS plasticization. This can be arisen from the supplemental out-of-plane shear and moment as shown in Fig. 5. As the slip-critical ultimate state governed the performance of the RBS model, the corresponding moment capacity can be derived by multiplying the interfacial pressure due to M_{bp} by the friction coefficient (μ), as follows:

$$M_{slip} = \mu\left(\frac{M_{bp}}{d}\right)d = 0.3 \times 320 = 96\ kN.m$$

Considering the multiplier $D_u = 1.13$ that reflects the ratio of the mean installed bolt pretension to the specified minimum bolt pretension as defined by AISC 360 [40], the slip-critical moment, M_{slip}, will be around 110-kN.m as shown in Fig. 4. It should be noted that the slip-critical moment for the positive case is approximately half of that in the negative case since there is only one row of resistant bolts.

References

[1] Rutherford & Chekene Consulting Engineers, Techniques for the Seismic Rehabilitation of Existing Buildings, FEMA 547, Federal Emergency Management Agency, Washington, 2006.

[2] A. Braconi, A. Tremea, G. Lomiento, N. Bonessio, F. Braga, B. Hoffmeister, M. Gundel, S. Karamanos, G. Varelis, R. Obiala, P. Tsintzos, D. Vassilikis, J. Lobo, P. Bartlam, S. Estanislau, L. Nardini, F. Morelli, W. Salvatore, D. Dubina, A. Dogariu, S. Bordea, G. Bortone, N. Signorini, G. Fianchisti, L. Fulop, Steel Solutions for Seismic Retrofit and Upgrade of Existing Constructions, Research Fund for Coal and Steel, European Comission, report B-1049, Brussels, Belgium, 2013.

[3] American Institute of Steel Construction AISC, Seismic Provisions for Steel Buildings, AISC, Chicago IL, US, 2022.

[4] Tsavdaridis K., Lau C., Alonso-Rodriguez A. (2025) Experimental behaviour of non-seismical RWS connections with perforated beams under cyclic actions, J. Constr. Steel Res.; 183 : 1–11.

[5] K.D. Tsavdaridis, T. Papadopoulos, A FE parametric study of RWS beam-to-column bolted connections with cellular beams, J. Constr. Steel Res. 116 (2016) 92–113.

[6] M.A. Shaheen, K.D. Tsavdaridis, S. Yamada, Comprehensive FE study of the hysteretic behaviour of steel-concrete composite and non-composite RWS beam-to-column connections, J. Struct. Eng. ASCE 144 (9) (2018).

[7] K. Boushehri, K.D. Tsavdaridis, G. Cai, Seismic behaviour of RWS moment connections to deep columns with European sections, J. Constr. Steel Res. 161 (2019) 416–435.

[8] F. Almutairi, K. The Tsavdaridis, Effect of degree of composite action on reduced web section (RWS) connections, in: The 9th European Conference on Steel and Composite Structures (EUROSTEEL 2021). 1–3 September, Sheffield, UK, 2021.

[9] S. Fares, J. Coulson, D. Dinehart, Castellated and Cellular Beam Design, American Institute of Steel Construction, AISC, Chicaco IL, 2017.

[10] R. Lawson, S. Hicks, Design of Composite Beams with Large Web Openings, The Steel Construction Institute, Berkshire UK, 2011.

[11] S. Mahin, Lessons from damage to steel buildings during the Northridge earthquake, Eng. Struct. 20 (4–6) (1998) 261–270.

[12] K.D. Tsavdaridis, C. Pilbin, C.K. Lau, FE parametric study of RWS/WUF-B moment connections with elliptically-based beam web openings under monotonic and cyclic loading, International Journal of Steel Structures 17 (2017) 677–694.

[13] K. Tsavdaridis, C. Lau, Extended end-plate RWS connections with perforated beams under cyclic loading, in: SECED 2019 Conference on Earthquake and Civil Engineering Dynamics. 9–10 September, 2019, Greenwich, London, UK, 2019.

[14] D.T. Naughton, K.D. Tsavdaridis, C. Maraveas, A. Nicolaou, Pushover analysis of steel seismic resistant frames with RWS and RBS connections, Front. Built Environ. (EPFL), Research Topic: Resilient Pre-Engineered Metal Based Connections - Accidental Effects and Design Aspects. 3 (2017), 59, https://doi.org/10.3389/fbuil.2017.00059.

[15] C. Uang, Q. Yu, S. Noel, Cyclic testing of steel moment connections rehabilitated with RBS or welded haunch, J. Struct. Eng. ASCE 126 (1) (2000) 57–68.

[16] A. Moslehi Tabar, A. Deylami, Instability of beams with reduced beam section moment connections emphasizing the effect of column panel zone, J. Constr. Steel Res. 61 (2005) 1475–1491.

[17] N. Fanaie, S.S. Faegh, F. Partovi, An improved and innovative formulation for calculating amplified elastic story drift induced by RBS connections in steel moment frames, J. Constr. Steel Res. 160 (2019) 510–527.

[18] M. Shariati, M. Ghorbani, M. Naghipour, N. Alinejad, A. Toghroli, The effect of RBS connection on energy absorption in tall buildings with braced tube frame system, Steel and Composite Structures, An International Journal 34 (3) (2020) 393–407.

[19] C.E. Sofias, D.T. Pachoumis, Assessment of reduced beam section (RBS) moment connections subjected to cyclic loading, Journal of Constructional Steel Research 171 (2020) 106151.

[20] K. Tsavdaridis, C. D'Mello, Web buckling study of the behaviour and strength of perforated steel beams with different novel web opening shapes, J. Constr. Steel Res 67 (10) (2011) 605:620.

[21] N. Fanaie, S. Kazerani, S. Soroushnia, Numerical study of slotted web drilled flange moment frame connection, Journal of Numerical Methods in Civil Engineering 1 (3) (2017) 16–23.

[22] R. Clough, J. Penzien, Dynamics of structures, 2nd Edition., Computers and Structures Inc, Walnut Creek, CA, 2010.

[23] T. Takeda, M. Sozen, N. Nielsen, Reinforced concrete response to simulated earthquakes, Journal of the structural division ASCE 96 (12) (1970).

[24] FEMA 356, Prestandard and commentary for the seismic rehabilitation of buildings, in: Federal Emergency Management Agency FEMA; Washington DC, 2000.

[25] Extended 3D Analysis of Building Systems vol. 16, Computer and Structures inc., Berkeley CA, 2018.

[26] D. Vamvatsikos, A. Cornell, Incremental dynamic analysis, Earthquake Engineering & Structural Dynamics 31 (3) (2001) 491–514.

[27] Applied Technology Council ATC, Next-Generation Performance-Based Seismic Design Guidelines, Federal Emergency Management Agency FEMA, Washington DC, 2006.

[28] F. Flores, D. García-Lopez, F. Charney, Assessment of floor accelerations in special steel moment frames, J. Constr. Steel Res. 106 (2015) 154–165.

[29] C. Del Gaudio, M. De Risi, G. Verdareme, Empirical drift-fragility functions and loss estimation for infills in reinforced concrete frames under seismic loading, Bull. Earthq. Eng. 17 (2019) 1285–1330.

[30] Applied Technology Council ATC, Quantification of Building Seismic Performance Factors. FEMA 695, Federal Management Agency, Washington DC, 2009.

[31] ANSI/AISC 360, Specification for Structural Steel Buildings, American Institute of steel Construction, Chicago, US, 2016.

[32] ASCE/SEI-7, Minimum Design Loads and Associated Criteria for Buildings and Other Structures, American Society of Civil Engineering, Virginia, US, 2016.

[33] A. Chopra, R. Goel, Building period formulas for estimating seismic displacements, Earthquake Spectra 16 (2) (2000) 533–536.

[34] A. Alimoradi, F. Naeim, Evolutionary modal identification utilizing coupled shear–flexural response—implication for multistory buildings, Part II: application. The structural design of tall and special buildings 15 (2006) 67–103.

[35] A. Chiozzi, E. Miranda, In plane fragility assessment of masonry infill panels, in: 16th European Conference on Earthquake Engineering; Thessaloniki, Greece, 2018.

[36] E. Gandelli, A. Taras, J. Distl, V. Quaglini, Seismic retrofit of hospitals by means of hysteretic braces: influence on acceleration-sensitive non-structural components, Front. Built Environ. 5 (2019), 100, https://doi.org/10.3389/fbuil.2019.00100.

[37] R. Alonso, E. Miranda, Assessment of building behavior under near-fault pulse-like ground motions through simplified models, Soil Dyn. Earthq. Eng. 79 (2015) 47–58.

[38] N. Kottegoda, R. Rosso, Applied Statistics for Civil and Environmental Engineers, 2nd edition, Wiley-Blackwell, Hoboken, NJ, 2008.

[39] ANSI/AISC 358, Prequalified Connections for Special and Intermediate Steel Moment Frames for Seismic Applications, Including Supplement No. 1, American Society of Civil Engineering, Chicago IL, US, 2016.

[40] AISC 360, Specification for Structural Steel Buildings, American Society of Civil Engineering, Chicago IL, US, 2016.